nature neuroscience

Neurometabolic coupling in cerebral cortex reflects synaptic more than spiking activity

Ahalya Viswanathan & Ralph D Freeman

In noninvasive neuroimaging, neural activity is inferred from local fluctuations in deoxyhemoglobin. A fundamental question of functional magnetic resonance imaging (fMRI) is whether the inferred neural activity is driven primarily by synaptic or spiking activity. The answer is critical for the interpretation of the blood oxygen level–dependent (BOLD) signal in fMRI. Here, we have used well-established visual-system circuitry to create a stimulus that elicits synaptic activity without associated spike discharge. In colocalized recordings of neural and metabolic activity in cat primary visual cortex, we observed strong coupling between local field potentials (LFPs) and changes in tissue oxygen concentration in the absence of spikes. These results imply that the BOLD signal is more closely coupled to synaptic activity.

BOLD fMRI has become a central tool in basic and applied neuroscience because it provides noninvasive maps of neural activation in the brain. However, the BOLD signal does not directly measure neural activity, but rather measures local fluctuations in deoxyhemoglobin (dHb) concentration[1–5]. As technological advances improve the spatial resolution of fMRI, it becomes increasingly important to quantify the relationship between the BOLD signal and the neural activity that it infers[6,7]. Specifically, it remains unclear whether the BOLD signal reflects mainly neuronal input (synaptic activity) or neuronal output (spiking activity). Using well-known properties of early visual pathways, we were able to dissociate these two measures to determine their relative contributions to changes in tissue oxygen.

Tissue oxygen is related to dHb through the oxygen-hemoglobin dissociation curve and the local oxygen concentration gradient in tissue. In addition, both the BOLD signal and tissue oxygen are similarly influenced by changes in cerebral blood volume (CBV), cerebral blood flow (CBF) and oxygen consumption (the cerebral metabolic rate of oxygen, $CMRO_2$)[8–10]. Therefore, it is reasonable to assume that changes in tissue oxygen are indicative of analogous changes in the BOLD signal. We have previously used a dual microelectrode (Unisense A/S) to make simultaneous colocalized extracellular measurements of tissue oxygen and neural activity in cerebral cortex[11]. This technique allows us to examine the neurometabolic coupling at a submillimeter level. The Clark-style polarographic oxygen sensor measures changes in oxygen tension, which is linearly related to tissue oxygen for the measured range[12]. These measurements are colocalized with simultaneous recordings of extracellular neuronal activity in the form of multi-unit spiking activity (MUA) and local field potentials (LFPs), which are commonly thought to measure synaptic activity[13–18]. An advantage of this method is the high resolution of the measurements that we can use to observe the effects of minor manipulations of a visual stimulus on the tissue oxygen response.

RESULTS

Temporal frequency tuning of tissue oxygen and LFPs

Our previous work focused on spatial properties of the visual stimulus. In the current study, we manipulated temporal characteristics to separate synaptic and spiking activity, as described below. To establish a basis for this comparison, we conducted a preliminary experiment to verify that temporal frequency tuning is present in both the tissue oxygen and LFP responses. Representative tissue oxygen, MUA and LFP responses in cat primary visual cortex (area 17) to stimuli at four temporal frequencies are illustrated (**Fig. 1**). The amplitude of the positive peak of the tissue oxygen responses ranged from 13.33% change for 20 Hz to 22.97% change for 4 Hz. MUA responses were band-pass filtered between 500 Hz and 8 kHz, with response strength determined by taking the mean evoked firing-rate and subtracting the spontaneous rate (mean firing-rate during 30–44-s interstimulus intervals). Mean measured MUA values ranged from 3.65 spikes per s for 20 Hz to 26.05 spikes per s for 4 Hz. LFP responses were low-pass filtered between 0.7 Hz and 170 Hz, with frequency bands defined as follows: δ (0.7–4 Hz), θ (4–8 Hz), α (8–12 Hz), β (12–25 Hz), γ_L (25–90 Hz), and γ_H (90–170 Hz). The frequency values for these bands were chosen on the basis of previous work[19,20]. Modulated power[20] was used as a measure of LFP response strength. Modulated power was calculated by taking the power at each frequency (mean over stimulus duration), dividing by the mean baseline power (1 s before stimulus onset), and summing over the frequency band. Summed modulated power in the gamma band (γ_L) extended from 67.32 dB for 20 Hz to 77.11 dB for 4 Hz.

Group in Vision Science, School of Optometry, Helen Wills Neurosciences Institute, University of California, Berkeley, California 94720-2020, USA. Correspondence should be addressed to R.D.F. (freeman@neurovision.berkeley.edu).

Received 15 May; accepted 14 August; published online 9 September 2007; doi:10.1038/nn1977

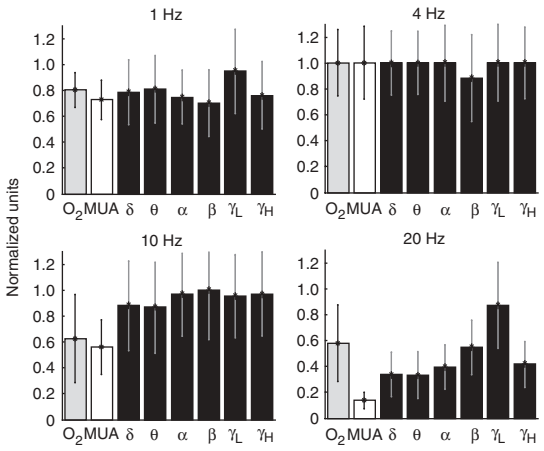

Figure 1 Temporal frequency tuning of tissue oxygen, MUA and LFP responses. Tissue oxygen, MUA and LFP signals (means across six sites ± 1 s.e.m) were normalized by the maximum response (mean across trials) across four temporal frequencies (1, 4, 10 and 20 Hz). Tissue oxygen responses (O_2) represent mean amplitude of the positive peak in percent change. MUA responses show mean firing rate during stimulus presentation minus mean spontaneous rate. LFP responses show modulated power summed over each frequency band: δ, θ, α, β, γ_L and γ_H.

There are two components to the tissue oxygen response (O_2 in **Fig. 1**). The initial negative component, or the initial dip, is thought to be associated with changes in $CMRO_2$[9,21], whereas the delayed positive component, or the positive peak, reflects changes in CBF[9,13,15]. A factor that must be considered in colocalized measurements of neural, vascular and metabolic responses is that they all occur at distinct spatial scales. We assumed that LFPs are collected over 2–3 mm^2 and MUA are collected over 300–800 μm^2 (refs. 22,23). Correspondingly, increases in CBF are thought to sum over an area of approximately 2 mm^2 (ref. 21), whereas changes in $CMRO_2$ appear to be localized to an area of approximately 200 μm^2 (ref. 11). Here, we quantified tissue oxygen responses by calculating the amplitude of the positive peak in percent signal change. This is based on the similar estimated spatial scales of CBF and LFP measurements.

Responses to the 1-Hz temporal frequency stimulus (**Fig. 1**) were robust for MUA, tissue oxygen and all LFP frequency bands. There were similarly strong responses across measures for the 4-Hz stimulus. This uniformity of response strength began to break down at higher temporal frequencies. At 10 Hz, there was slight attenuation of the MUA response and increased variability in the strength of the tissue oxygen response. Here, the responses at the α to γ_H frequency bands (8–170 Hz) were significantly higher than both tissue oxygen and MUA responses (*t*-test, $P = 0.025$–0.0497; β responses were not significantly different from tissue oxygen, *t*-test, $P = 0.0513$). The differences became more pronounced at 20 Hz, when the MUA response was strongly attenuated, as were responses in the lower LFP frequency bands. However, both tissue oxygen and gamma band (γ_L) responses remained strong. This is consistent with previous work in which LFP temporal frequency tuning was examined[24]. For these sites, coupling between tissue oxygen and gamma band activity is independent of temporal frequency, unlike the relationship between tissue oxygen and MUA.

Dissociation of spiking and synaptic activity

Having established the presence of temporal frequency tuning in both tissue oxygen and LFP responses, we conducted experiments that permit dissociation of spiking and synaptic activity. Our approach relied on the established observation that neurons in the early visual pathway (lateral geniculate nucleus, LGN) are tuned to higher temporal frequencies than those in visual cortex[25]. Cortical layers 4 and 6 receive direct input from LGN. Although intracortical connections are also present in these layers, we assumed a predominance of LGN input[26]. This means that gross extracellular potentials will reflect a prevalence of synaptic over spiking activity for high temporal frequency stimuli. An additional advantage of varying temporal frequency versus other visual parameters concerns cortical maps. Although orientation and spatial frequency maps have been identified[27,28], no equivalent structure has been found for temporal frequency. This suggests a uniform spread of neural activation across a range of temporal frequencies.

For our experiments, we used binocular full-field (60°) drifting sinusoidal gratings presented at 100% contrast as stimuli. The gratings had a spatial frequency of 0.2 cycles $degree^{-1}$, with preferred orientation being determined by peak MUA tuning. We used three test conditions: low temporal frequency (2 or 4 Hz depending on peak MUA tuning), high temporal frequency (30 Hz, based on refresh rate of stimulus presentation monitor) and null (no stimulus). Significant tissue oxygen responses (*t*-test, $1.00 \times 10^{-16} \leq P \leq 0.0028$; 24 out of 26 values, $P < 0.0005$) were found at 13 sites. We observed neuronal spiking, with a strong MUA response to the 4-Hz stimulus and no response to the 30-Hz stimulus (**Fig. 2a**). Conversely, there were clear tissue oxygen responses to both the 4-Hz and 30-Hz stimuli. As expected, both the tissue oxygen and MUA responses to the null condition were identical to the baseline signals, or noise.

The LFP spectrograms (**Fig. 2b**) showed modulated signal power as a function of frequency and time. There was a marked increase in signal power across frequency bands in response to the 4-Hz stimulus, although the strength of the response weakened after the first second of stimulus presentation. In response to the 30-Hz stimulus, the initial increase in signal strength was slightly weaker than that for the 4-Hz stimulus, particularly in the gamma and high gamma bands. However, although signal strength varied with time, there was also a clear increase

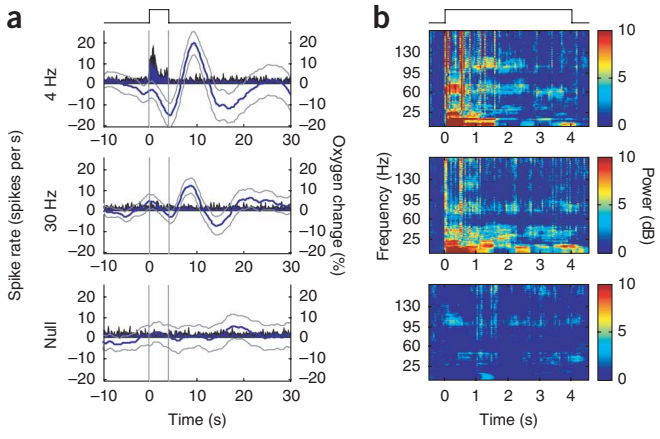

Figure 2 Example recording site of responses to large (60°) stimulus. (**a**) Spike-time histograms (dark blue area) and oxygen responses were averaged across 32 trials. Solid gray lines surrounding oxygen responses (solid blue lines) show ± 1 s.e.m. (**b**) LFP spectrograms were calculated by taking the mean signal modulated power across trials. Responses are shown for 4-Hz and 30-Hz stimuli and a null stimulus. Stimuli were binocularly presented drifting sine-wave gratings with 4-s stimulus duration, as depicted by the vertical gray lines in **a** and by the step functions at the top of **a** and **b**.

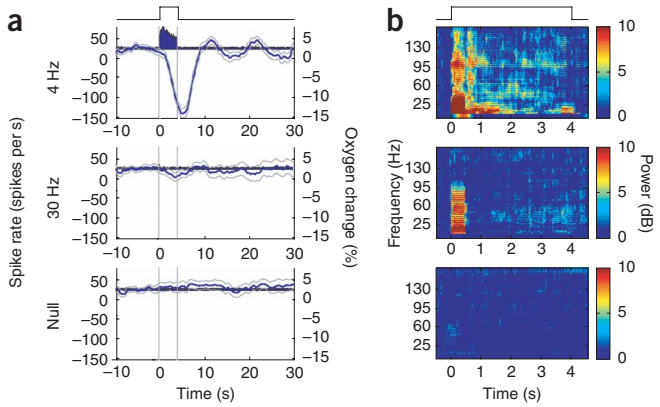

Figure 3 Response to small stimulus at high spatial frequency. (**a**) Spike-time histograms (dark blue area) and oxygen responses (solid blue lines) were averaged across 48 trials. (**b**) LFP spectrograms were calculated as in **Figure 2**. Stimuli were identical to those in **Figure 2**, except that the stimulus was presented over 10° of visual area (centered over the receptive field as determined by peak MUA activity), at a spatial frequency of 0.7 cycles degree^{-1}.

in signal power throughout the stimulus duration for this condition, especially for frequencies below 50 Hz. Like the tissue oxygen and MUA responses, the LFP spectrogram for the null condition showed baseline noise, but no stimulus-induced effect.

Responses to small stimuli

To explore the relative contributions of LGN afferents and recurrent feedback from area 18 to the tissue oxygen response, we tested four additional recording sites with visual stimuli at higher spatial frequencies (0.5–0.7 cycles degree^{-1}). In addition, we used smaller stimuli at these sites to decrease the possibility that tissue oxygen responses were a result of MUA activity outside of our electrode's field of view (**Fig. 3**). Like responses to the larger stimuli, there was a strong MUA response to the 4-Hz stimulus, but no increases in MUA were observed for the 30-Hz or null conditions. As expected from previous work, the tissue oxygen responses to these small stimuli differed from those evoked by larger stimuli[20]. For the 4-Hz stimulus, the tissue oxygen response was primarily composed of a strong initial dip. There was also a small, but significant (*t*-test, $P = 8.09 \times 10^{-8}$), initial dip response to the 30-Hz stimulus. Both the 4-Hz and 30-Hz tissue oxygen responses were also significantly different from the null condition (*t*-test, $P = 6.58 \times 10^{-8}$ and $P = 2.64 \times 10^{-12}$, respectively). These observations are consistent with the expectation that a small stimulus elicits a highly localized change in neural and metabolic activity. We have previously shown that the initial dip is largest at sites producing the strongest neural responses[11]. Here, the absence of MUA implies that the initial dip is tied to the concurrent increase in LFP power.

There were strong initial LFP responses to both the 4-Hz and the 30-Hz stimuli (**Fig. 3b**). The 4-Hz response decreased in strength 500 ms following stimulus onset, but maintained a strong increase in power across frequencies throughout stimulus duration. The 30-Hz response also decreased 500 ms after stimulus onset, but this decrease in power was more severe than for the 4-Hz condition, and very weak increases in power between 25 and 60 Hz were observed for the remainder of stimulus duration.

LFP responses by frequency band

We analyzed the LFP response across all 17 recording sites, with summed LFP power being determined by taking the sum of modulated LFP power over stimulus duration for each frequency band (**Fig. 4**). As observed above (**Figs. 2** and **3**), the LFP response was weaker for the 30-Hz stimulus than for the low temporal frequency stimuli of either 2 or 4 Hz. However, responses to both types of stimuli are similar in that there was a strong response for frequencies between 25 and 60 Hz (the lower portion of the gamma band). These findings are consistent with previous work reporting high correlations between gamma band activity and the BOLD signal[14,18,20,23,29]. The relative decrease in signal strength for gamma frequencies above 60 Hz supports the theory of a distinction between a lower and an upper gamma band. Recent work in primary visual cortex has also shown stronger responses in the lower portion of the gamma band (30–50 Hz)[29]. This is notable, considering the large amount of variability in the definition of the gamma band[14,18,20,23,29]. Our results suggest that the lower portion of the gamma band (25–60 Hz) is more closely tied to synaptic activity than higher LFP frequencies.

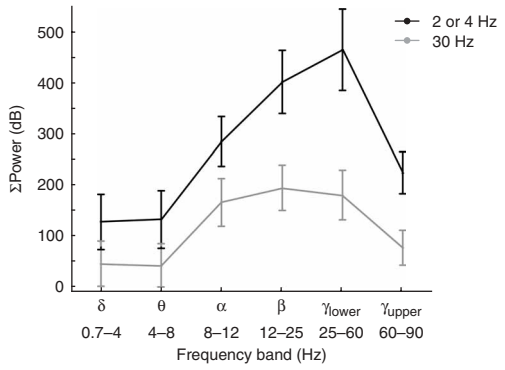

Figure 4 Population data: mean LFP responses across sites. LFP responses ($n = 17$) were quantified by summing modulated power over each frequency band. The solid black line depicts the mean response across sites to the low temporal frequency condition (either 2 or 4 Hz depending on peak spike tuning) minus the mean null response. The solid gray line shows the mean response to the high temporal frequency condition (30 Hz) minus the mean null response. Error bars represent ± 1 s.e.m across sites.

DISCUSSION

Previous attempts to address the question of whether the BOLD signal is more closely tied to spiking or synaptic activity have relied on comparisons via correlation coefficients[17,18]. These analyses have led to similar correlation values for both neural variables, that is, MUA versus BOLD and LFPs versus BOLD. Because there is also a high correlation between MUA and LFPs, these results are difficult to interpret. We avoid this problem by dissociating the two types of neural activity.

Although our results indicate that lower gamma band (25–60 Hz) activity is most closely tied to the tissue oxygen response, we also observed stimulus-dependent responses in other frequency bands. Both types of stimuli (low and high temporal frequency) also elicited strong responses in the α and β bands. β activity has previously been strongly correlated to γ-band activity[24], although its functional role is not clear. High LFP power has also been found in the α band in response to visual stimuli at high contrast[20]. As our stimuli were presented at 100% contrast, it is not surprising that we also found high LFP power in the α band. Also of note is the relative strength of α-band power for the 30-Hz responses. Recent work has associated α-band activity with top-down inhibitory processes[30,31]. This is consistent with the theory that high temporal frequency information from LGN is subject to

intracortical inhibition in primary visual cortex[25,32], and could explain the prevalence of α-band activity in response to high temporal frequency stimuli.

Here, we demonstrate recording sites in the visual cortex at which a spiking response is not necessary for stimulus-induced changes in tissue oxygen. We also observed that sites showing this behavior had strong LFP responses in the lower portion of the γ frequency band. Together, these findings indicate that changes in tissue oxygen are more closely coupled with LFPs than with neuronal spikes. By extrapolation, our results suggest that the BOLD fMRI signal primarily reflects synaptic, rather than spiking, activity.

METHODS

Animal preparation. Animal procedures were conducted in compliance with the US National Institutes of Health *Guide for the Care and Use of Laboratory Animals*. Mature cats were initially anesthetized using 1.5–3% isoflurane gas. Core body temperature was maintained at 38 °C. Following cannulation of forepaw femoral veins, isoflurane was discontinued and anesthesia was maintained with continuous intravenous infusion of fentanyl (10 μg per kg of body weight h^{-1}) and thiopentothal sodium (6 mg per kg h^{-1}). A tracheotomy was carried out, and the animal was placed on artificial respiration with a mixture of 25% oxygen gas and 75% nitrous oxide. Electroencephalography, electrocardiogram, core body temperature, intratracheal pressure and expired CO_2 were monitored for the duration of the experiment. Area 17 craniotomies were carried out with center Horsley-Clarke coordinates of P4 L2, and the dura mater was removed to allow electrode penetration. Paralysis was induced with pancuronium bromide (0.2 mg per kg h^{-1}). During recording, the respiration rate was adjusted between 14 and 23 strokes min^{-1} to maintain expired CO_2 levels between 33 and 39 mm Hg.

Recording sites. All recordings were made using a Unisense A/S 3000 APOX probe. We were unable to determine cortical depth via histology, as lesions cannot be made with this device. Therefore, all depth measurements are based on micromanipulator readings. The electrode was initially advanced 500 μm below the cortical surface in area 17. The site was then tested for an adequate neuronal spiking response (>8 spikes per s). Sites without adequate visually driven spike rates were not included in the data analysis. On completion of all stimulus repetitions at a particular site, the electrode was advanced another 200 μm and the process of searching for sites in 100-μm increments was repeated.

Visual stimuli. Visual stimuli were binocularly presented full-field sine wave gratings displayed on a cathode ray tube (CRT) monitor (50 cd m^{-2} mean luminance) at a spatial frequency of 0.2 cycles $degree^{-1}$. Temporal frequency values were varied as described in the main text. The high temporal frequency value was 30 Hz, a value limited by the refresh rate of the CRT stimulus-presentation monitor. All stimuli were shown at 100% luminance and 100% contrast. Stimuli were also presented at optimal orientations, as determined by peak MUA tuning in the dominant eye. Interstimulus intervals varied between 30 and 44 s, with 16–88 repetitions.

Data analysis. Neural signals were filtered using a preamplifier. MUA was band-pass filtered between 500 Hz and 8 kHz at a sampling rate of 25 kHz. An arbitrary threshold was set just above the spontaneous response to the mean gray luminance background and all spikes collected about this threshold were considered to be part of MUA. LFPs were low-pass filtered from 0.7 to 170 Hz at a sampling rate of 500 Hz. To graphically interpret the LFP data, responses for each stimulus condition (averaged across trials) were converted to spectrograms using Slepian tapers with 500-ms windows and a 50-ms step size[20]. Noise removal was accomplished with a 60-Hz notch filter and a Matlab utility (rmlinesc.m, Chronux toolbox) used at the refresh rate of the stimulus CRT (78 or 85 Hz).

Statistical analysis. Tissue oxygen signals were preprocessed to maximize visibility of responses[11]. Because of low frequency oscillations, sites without significant tissue oxygen responses were not included. The significance of tissue oxygen responses was determined using Student's *t*-tests comparing tissue oxygen signals 5–15 s following stimulus onset to the 10-s prestimulus baseline. This test was chosen to examine whether the tissue oxygen signal following stimulus onset differed from baseline oscillations. A second measure of response strength compared the response amplitude with maximum amplitude of the baseline oscillations. For large and small stimulus sites, response amplitudes were determined by the positive peak and the initial dip, respectively. Responses with amplitudes less than 2 s.d. of the baseline period were not included.

ACKNOWLEDGMENTS

We thank Unisense A/S for continued collaboration in developing the combined sensor, J. Thompson for helpful comments during the conception of the project, P. Mitra and H. Bokil for assistance with LFP analysis, E. Allen and B. Pasley for helpful discussions, and B. Li for help with surgical preparation. This work was supported by research and CORE grants from the US National Eye Institute (EY01175 and EY03716) and a US National Science Foundation Graduate Research Fellowship (A.V.).

AUTHOR CONTRIBUTIONS

A.V. conducted the experiments and data analysis. Both A.V. and R.D.F. discussed the results and wrote portions of the manuscript.

Published online at http://www.nature.com/natureneuroscience
Reprints and permissions information is available online at http://npg.nature.com/reprintsandpermissions

1. Bandettini, P.A., Wong, E.C., Hinks, R.S., Tikofsky, R.S. & Hyde, J.S. Time course EPI of human brain function during task activation. *Magn. Reson. Med.* **25**, 390–397 (1992).
2. Ogawa, S. *et al.* Intrinsic signal changes accompanying sensory stimulation: functional brain mapping with magnetic resonance imaging. *Proc. Natl. Acad. Sci. USA* **89**, 5951–5955 (1992).
3. Kwong, K.K. *et al.* Dynamic magnetic resonance imaging of human brain activity during primary sensory stimulation. *Proc. Natl. Acad. Sci. USA* **89**, 5675–5679 (1992).
4. Kim, S.G. & Ugurbil, K. Functional magnetic resonance imaging of the human brain. *J. Neurosci. Methods* **74**, 229–243 (1997).
5. Logothetis, N.K. & Wandell, B.A. Interpreting the BOLD signal. *Annu. Rev. Physiol.* **66**, 735–769 (2004).
6. Duong, T.Q., Kim, D.S., Ugurbil, K. & Kim, S.G. Localized cerebral blood flow response at submillimeter columnar resolution. *Proc. Natl. Acad. Sci. USA* **98**, 10904–10909 (2001).
7. Kim, D.S. *et al.* Spatial relationship between neuronal activity and BOLD functional MRI. *Neuroimage* **21**, 876–885 (2004).
8. Zheng, Y. *et al.* A model of the hemodynamic response and oxygen delivery to the brain. *Neuroimage* **16**, 617–637 (2002).
9. Thompson, J.K., Peterson, M.R. & Freeman, R.D. Separate spatial scales determine neural activity–dependent changes in tissue oxygen within central visual pathways. *J. Neurosci.* **25**, 9046–9058 (2005).
10. Offenhauser, N., Thomsen, K., Caesar, K. & Lauritzen, M. Activity-induced tissue oxygenation changes in rat cerebellar cortex: interplay of postsynaptic activation and blood flow. *J. Physiol. (Lond.)* **565**, 279–294 (2005).
11. Thompson, J.K., Peterson, M.R. & Freeman, R.D. Single-neuron activity and tissue oxygenation in the cerebral cortex. *Science* **299**, 1070–1072 (2003).
12. Fatt, I. *Polarographic Oxygen Sensors* 197–218 (CRC Press, Cleveland, Ohio, 1976).
13. Mathiesen, C., Caesar, K., Akgoren, N. & Lauritzen, M. Modification of activity-dependent increases of cerebral blood flow by excitatory synaptic activity and spikes in rat cerebellar cortex. *J. Physiol. (Lond.)* **512**, 555–566 (1998).
14. Logothetis, N.K., Pauls, J., Augath, M., Trinath, T. & Oeltermann, A. Neurophysiological investigation of the basis of the fMRI signal. *Nature* **412**, 150–157 (2001).
15. Caesar, K., Thomsen, K. & Lauritzen, M. Dissociation of spikes, synaptic activity, and activity-dependent increments in rat cerebellar blood flow by tonic synaptic inhibition. *Proc Natl Acad Sci. USA* **100**, 16000–16005 (2003).
16. Devor, A. *et al.* Coupling of total hemoglobin concentration, oxygenation, and neural activity in rat somatosensory cortex. *Neuron* **39**, 353–359 (2003).
17. Mukamel, R. *et al.* Coupling between neuronal firing, field potentials, and fMRI in human auditory cortex. *Science* **309**, 951–954 (2005).
18. Niessing, J. *et al.* Hemodynamic signals correlate tightly with synchronized gamma oscillations. *Science* **309**, 948–951 (2005).
19. Logothetis, N.K. The underpinnings of the BOLD functional magnetic resonance imaging signal. *J. Neurosci.* **23**, 3963–3971 (2003).
20. Henrie, J.A. & Shapley, R. LFP power spectra in V1 cortex: the graded effect of stimulus contrast. *J. Neurophysiol.* **94**, 479–490 (2005).
21. Malonek, D. & Grinvald, A. Interactions between electrical activity and cortical microcirculation revealed by imaging spectroscopy: implications for functional brain mapping. *Science* **272**, 551–554 (1996).
22. Kreiman, G. *et al.* Object selectivity of local field potentials and spikes in the macaque inferior temporal cortex. *Neuron* **49**, 433–445 (2006).

23. Liu, J. & Newsome, W.T. Local field potential in cortical area MT: stimulus tuning and behavioral correlations. *J. Neurosci.* **26**, 7779–7790 (2006).
24. Rager, G. & Singer, W. The response of cat visual cortex to flicker stimuli of variable frequency. *Eur. J. Neurosci.* **10**, 1856–1877 (1998).
25. Hawken, M.J., Shapley, R.M. & Grosof, D.H. Temporal-frequency selectivity in monkey visual cortex. *Vis. Neurosci.* **13**, 477–492 (1996).
26. Gilbert, C.D. Laminar differences in receptive field properties of cells in cat primary visual cortex. *J. Physiol. (Lond.)* **268**, 391–421 (1977).
27. Vanzetta, I. & Grinvald, A. Increased cortical oxidative metabolism due to sensory stimulation: implications for functional brain imaging. *Science* **286**, 1555–1558 (1999).
28. Issa, N.P., Trepel, C. & Stryker, M.P. Spatial frequency maps in cat visual cortex. *J. Neurosci.* **20**, 8504–8514 (2000).
29. Wilke, M., Logothetis, N.K. & Leopold, D.A. Local field potential reflects perceptual suppression in monkey visual cortex. *Proc Natl Acad Sci. USA* **103**, 17507–17512 (2006).
30. von Stein, A., Chiang, C. & Konig, P. Top-down processing mediated by interareal synchronization. *Proc Natl Acad Sci. USA* **97**, 14748–14753 (2000).
31. Jokisch, D. & Jensen, O. Modulation of gamma and alpha activity during a working memory task engaging the dorsal or ventral stream. *J. Neurosci.* **27**, 3244–3251 (2007).
32. Maex, R. & Orban, G.A. Model circuit of spiking neurons generating directional selectivity in simple cells. *J. Neurophysiol.* **75**, 1515–1545 (1996).